

## **Correlation between Critical Pitting Temperature and Degree of Sensitization of UNS S32750 Duplex Stainless Steel Corrosion**

*M. Sun<sup>1</sup>, L. He<sup>1,\*</sup>, X.Q. Li<sup>1</sup>, P. Li<sup>1</sup>*

School of Materials Engineering, Shanghai University of Engineering Science, Shanghai 201620, China

\*E-mail: [jlljhl@163.com](mailto:jlljhl@163.com)

*Received: 7 October 2019 / Accepted: 19 November 2019 / Published: 31 December 2019*

---

This study aims to explore the correlation of critical pitting temperature (CPT) and degree of sensitization (DOS) for UNS S32750 duplex stainless steel after being exposed to different heat conditions. Both the CPT and DOS are strongly dependent on the microstructure. It is also revealed that the pitting resistance heals after prolonging the ageing time, but the degree of sensitization continues to increase.

---

**Keywords:** Duplex Stainless Steel, Pitting Corrosion, Intergranular Corrosion, CPT, DOS

### **1. INTRODUCTION**

Duplex stainless steels (DSS) have excellent mechanical properties and corrosion resistance due to their representative two-phase structures and have been widely used in many aspects of production and manufacturing, such as nuclear, chemical, marine and petrochemical production [1]. However, duplex stainless steel inevitably suffers from heat conditions that lead to precipitation of various intermetallic phases and compounds. Accompany the precipitation of these Cr- and Mo-rich phases, Cr- and Mo-depleted zones are then produced, which induce the corrosion resistance deterioration of the alloy, especially the pitting and intergranular corrosion resistance properties [2].

Pitting corrosion is a very damaging corrosion type for steel that may cause a major failure in industrial applications [3]. It is generally accepted that a medium temperature is one of the most important factors in pitting corrosion. Based on this, the concept of a critical pitting temperature was introduced by Brigham and Tozer [4]. The CPT test technique, based on recording the function of current response and media temperature in the studied system at an applied constant potential, has been widely used as an effective method for evaluating the pitting resistance of stainless steel.

Duplex stainless steels are quite susceptible to intergranular corrosion when they suffer thermal

cycling at 500-900 °C [5]. The precipitation of Cr- and Mo-rich phases at the two-phase interface and grain boundaries often leads to a generation of Cr-depleted zones that are easily corroded. Many test methods has been developed to determine the degree of sensitization or the susceptibility of the material to intergranular corrosion, including acid medium immersion test [6], eddy current testing [7], dynamic electrochemical impedance spectroscopy (DEIS) [8], electrochemical noise (EN) [9], single loop electrochemical potentiokinetic reactivation (SL-EPR) and double loop electrochemical potentiokinetic reactivation (DL-EPR) [10,11], etc. Among these methods, DL-EPR analytical method, due to its fast, quantitative and independent of the surface finish features, has been widely used to characterize the degree of sensitization of stainless steels [12].

Duplex stainless steel UNS S32750 as a high alloy concentration (Cr, Mo, N, etc.) super DSS possesses outstanding corrosion resistance and remarkable mechanical properties [13,14] and has excellent application potential for products under extremely harsh conditions [15]. However, the high alloy concentration also means greater precipitation tendencies and more complex precipitation mechanisms [16,17]. Despite many previous studies on the effect of phases on the corrosion behaviour of DSS, research on the correlation of critical pitting temperature and intergranular corrosion sensitivity of steel has rarely been conducted.

This paper investigates the microstructure evolution and corrosion behaviour of super duplex stainless steel UNS S32750 under different thermal cycling conditions. The pitting resistance of the materials is investigated by measuring the critical pitting temperature with potentiostatic polarization. Double-loop potentiodynamic reactivation (DL-EPR) is used to evaluate the degree of sensitization of the materials. The effects of different sensitization treatments on the corrosion behaviour of UNS S32750 and the relevance between the critical pitting temperature and the degree of sensitization are discussed.

## 2. EXPERIMENTAL

### 2.1 Materials and heat treatment

The chemical composition of an as-received hot-rolled UNS S32750 DSS sheet is listed in Table 1 and is used for all experiments. The stainless steel plates were cut into 12×12×2 mm blocks, annealed at 1080 °C for 1 h and then quenched in water to homogenize the structures. The specimens were aged at 900 °C for different holding times of 10 min, 30 min, 1 h, 2 h, 4 h, 10 h, 20 h, and 100 h, followed by water quenching. Throughout the heat treatment process, protective argon gas was continuously supplied.

**Table 1.** Chemical composition (wt.%) of UNS S32750.

Element	C	Cr	Ni	Mo	P	Si	Mn	N	S	Cu	Fe
wt. %	0.022	25.15	6.74	3.43	0.029	0.37	0.70	0.27	0.002	0.13	Bal.

## 2.2 Microstructural characterization

To identify the phase and precipitate distributions of the heat treatment specimens, they were mounted, polished and chemically etched in Behera reagent (20 mL HCl, 80 mL distilled water and 0.3 g  $K_2S_2O_5$ ) for 30-40 s at room temperature. A HITACHI S-3400 scanning electron microscope (SEM) with an attached GENESIS EDAX detector for energy dispersive spectroscopy (EDS) was applied to observe the surface layer of the specimens and the corrosion morphology of the specimens after electrochemical experiments.

In addition, the phase identification was conducted with a D8 Advance Bruker X-ray diffractometer (XRD) using a Co  $K\alpha$  radiation source with a scan range of  $10^\circ < 2\theta < 100^\circ$ .

Transmission electron microscopy (TECNAI G2 F20, FEI Inc.) equipped with an X-ray energy dispersive spectrometer (EDS) was conducted to identify tiny precipitates. Thin foil for TEM observation was cut from heat-treated specimens and further reduced to 50  $\mu\text{m}$  using GATAN PIPS II equipment for ion thinning.

## 2.3 Electrochemical measurements

All electrochemical tests were performed in a traditional three-electrode electrochemical cell. A CHI660E electrochemical workstation was used with the mounted and polished specimens, with an exposed region of  $10 \times 10$  mm, as the working electrodes, a platinum foil as the auxiliary electrode and a saturated calomel electrode (SCE) as the reference electrode.

The CPT measurements were carried out in a 1 mol/L NaCl solution. Prior to each measurement, the working electrode was cathodically polarized at -0.9 V/SCE for 120 s to eliminate oxides on the surface of the specimens, and then the open circuit potential ( $E_{OCP}$ ) was tested until the system was stable. Then, an anodic constant potential of 800 mV/SCE was applied, and the solution temperature was controlled to increase at a rate of  $1 \pm 0.1$   $^\circ\text{C}/\text{min}$  until the current density exceeded  $100 \mu\text{A}/\text{cm}^2$ . The temperature associated with a  $100 \mu\text{A}/\text{cm}^2$  current density was chosen as the criterion for CPT assessment [2]. Half an hour before the test, argon gas is applied to the solution to expel any dissolved oxygen, and the argon gas flow continues until completion of the experiment. The testing was repeated at least three times to ensure its reproducibility and reliability.

Double loop electrochemical potentiokinetic reactivation (DL-EPR) was applied to evaluate the intergranular corrosion (IGC) susceptibility of duplex stainless steels UNS S32750 [18]. The tests were carried out in a mixed solution of 2 M  $\text{H}_2\text{SO}_4$  + 1.5 M HCl, and the temperature was controlled to be  $35 \pm 1$   $^\circ\text{C}$ . The oxidation film of the specimens was removed in the same manner as the CPT test procedure. After the system was stable, the potential scan began from slightly below the open circuit potential ( $E_{OCP}$ ) to 0.4  $\text{V}_{\text{SCE}}$  at a scanning rate of 1.5 mV/s with a reverse sweep to the original potential at the same sweep rate. The DOS of IGC is defined by the following formula [19]:

$$R_a = \frac{I_r}{I_a} \times 100 \%$$

where  $I_a$  is the peak value of the activation current density and  $I_r$  is the peak value of the reactivation current density [20].

### 3. RESULTS AND DISCUSSION

#### 3.1 Microstructural analysis

Fig. 1 shows the XRD results of UNS S32750 aged at 900 °C for different times. For the as-annealed specimens, only diffraction peaks of the ferrite and austenite phase can be found. The diffraction peak of precipitates cannot be detected even for specimens aged for 2 h, which is attributed to the detection limit of XRD. With an extension of ageing time, the peak strength of the  $\gamma$  phase and  $\sigma$  phase gradually increase, while the peak of the  $\alpha$  phase continues to weaken, which means a clear eutectoid transformation takes place:  $\alpha \rightarrow \sigma + \gamma_2$  [21]. After ageing for 100 h, the eutectoid reaction is transformed almost completely, and most of the ferrite is transformed into  $\gamma_2$  and  $\sigma$  phases. This corresponds to the weak peak of the  $\alpha$  phases, the main peaks of the  $\gamma$  and  $\sigma$  phases were strengthened.

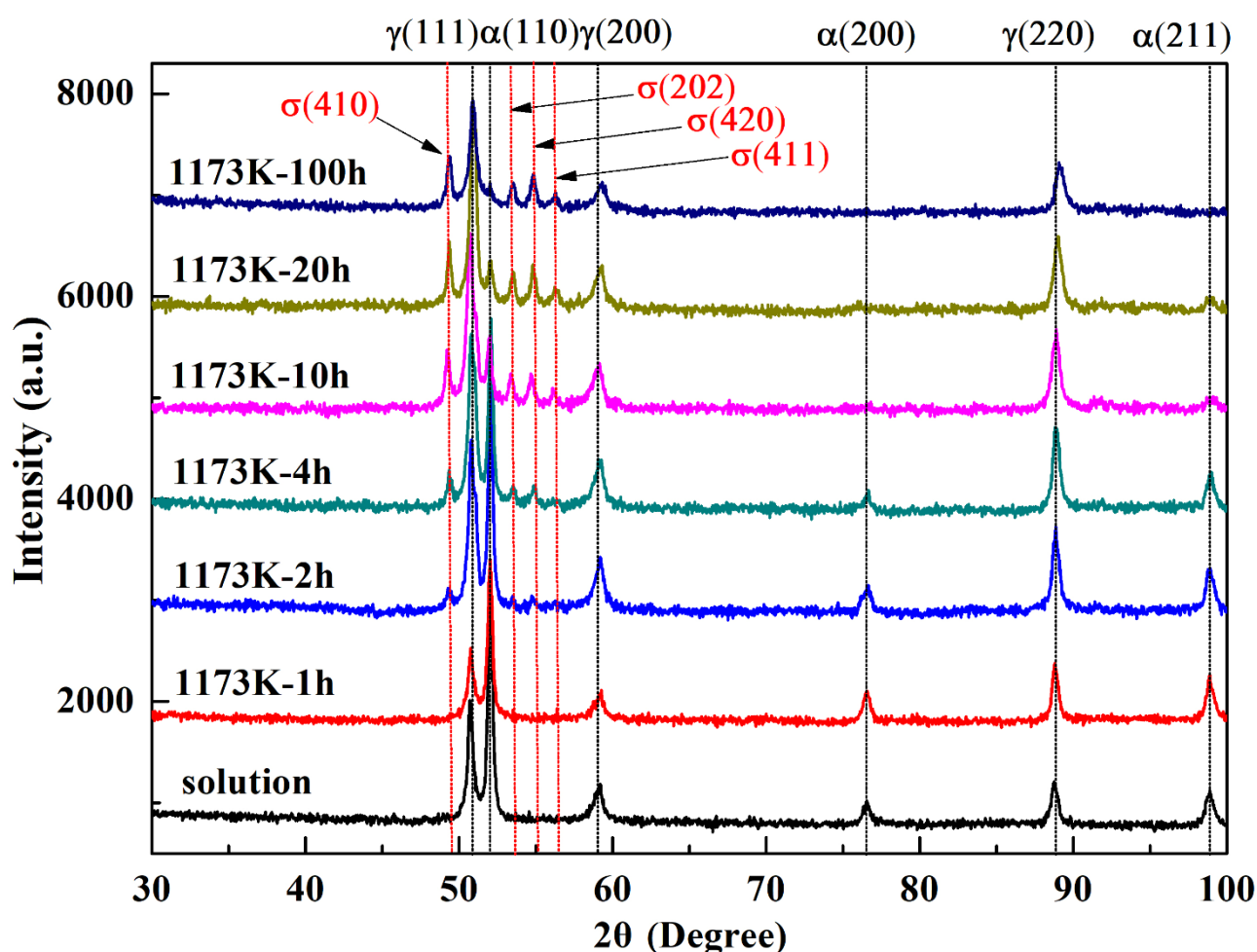


**Figure 1.** XRD results of the UNS S32750 specimens aged at 900 °C for various times.

Fig. 2 shows SEM micrographs of the duplex stainless steel UNS S32750 materials isothermally aged at 900 °C for different durations. A typical  $\alpha/\gamma$  two-phase structure can be observed for solution treated specimens; the  $\alpha/\gamma$  phase boundary is smooth, and no other precipitates emerge, as shown in Fig. 2(a). After ageing at 900 °C for 10 min, some precipitates emerge at the  $\alpha/\gamma$  phase interfaces, and the grain boundaries become coarse (Fig. 2(b)), owing to a low degree of atomic matching and high grain

boundary energy. As depicted in Fig. 2(c), when the ageing time is up to 30 min, a small dimension of  $\sigma$  phase can be observed. With an extension of ageing time, the  $\sigma$  phase grows up gradually, as shown in Fig. 2(d-g). The  $\sigma$  phase forms at crystal boundaries and has a tendency to grow up towards the  $\alpha$  phase, which can be attributed to the fact that  $\alpha$  is a thermodynamically unstable phase at 900 °C. The  $\sigma$  phase is chromium-rich and forms a chromium-depleted region adjacent to it; this further promotes the formation of  $\gamma_2$ , which is poor in chromium and rich in nitrogen [22,23]. The composition gradient of the chromium element provides the driving force for this transformation, which further broadens the chromium-depleted zones and makes the grain boundary continue to move towards the  $\alpha$  phase [24]. As shown in Fig. 2(h), the  $\sigma$  and  $\gamma_2$  phases continue to increase and grow up as the ageing time increases, while the volume fraction of the  $\alpha$  phase continues to decrease. When the ageing time reaches 100 h, most of the ferrite phase has transformed, which is difficult to distinguish by SEM (Fig. 2(i)), and this result is consistent with the results from the XRD test.

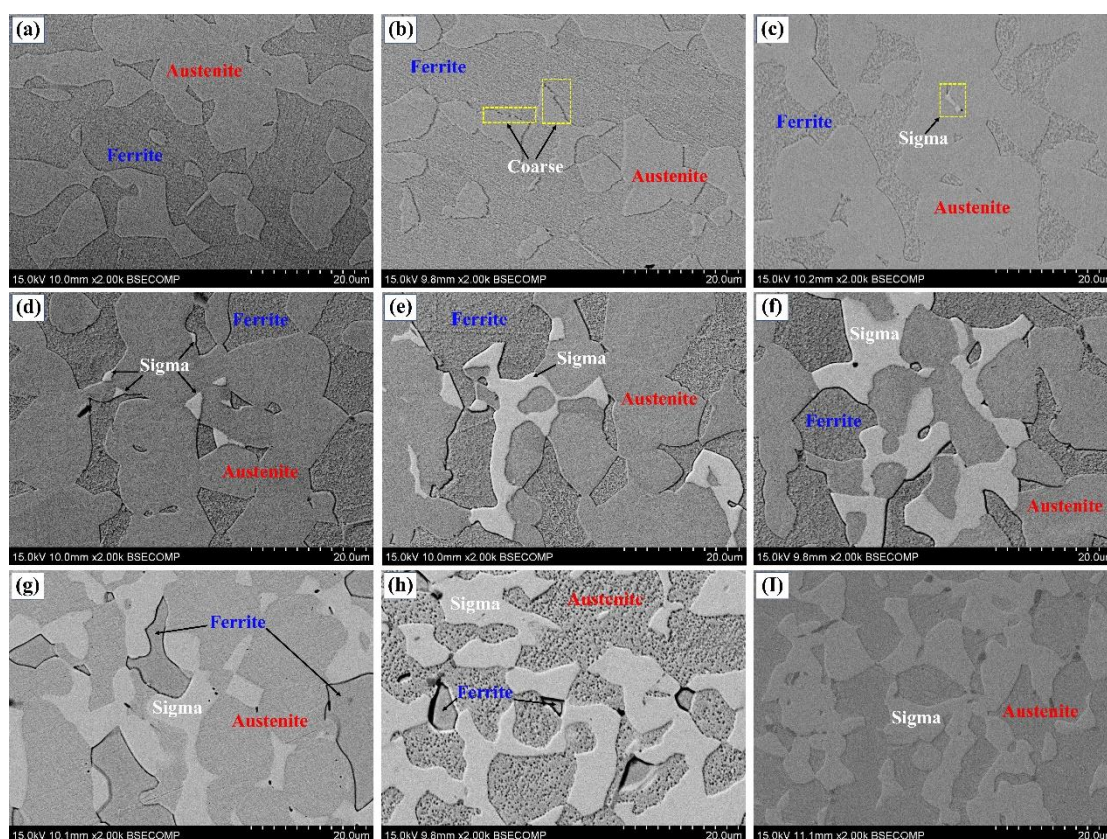


**Figure 2.** SEM-BSE micrographs of UNS S32750 specimens aged at 900 °C for (a) 0 min, (b) 10 min, (c) 30 min, (d) 1 h, (e) 2 h, (f) 4 h, (g) 10 h, (h) 20 h, and (i) 100 h.

To further identify the fine precipitates, TEM tests were carried out, and some precipitates, such as nitride ( $\text{Cr}_2\text{N}$ ), carbides ( $\text{M}_{23}\text{C}_6$ ), sigma phase ( $\sigma$ ) and secondary austenite phases ( $\gamma_2$ ), were detected. Fig. 3(a-c) shows the high-magnification TEM image of precipitates in specimens aged at 900 °C for 10 h. The calibration diagram of selected area electron diffraction (SAED) corresponding to the precipitates is shown in Fig. 3(d). It can be found from the figure that  $\sigma$  phase chromium-rich intermetallic

compounds, with a size of approximately several hundred nanometers, are preferentially precipitated at the  $\alpha/\gamma$  phase boundary. Furthermore, a concomitant secondary austenite is attached to the primary austenite phase and grows towards the direction of the  $\alpha$  phase. In addition, the precipitated phases of  $\text{Cr}_2\text{N}$  and  $\text{M}_{23}\text{C}_6$  can also be observed; though the precipitates originate from the  $\alpha/\gamma$  interface, with the formation of the secondary austenite, the new  $\alpha/\gamma$  interface gradually moves in the direction of ferrite. The chemical compositions of these precipitates were analysed by EDS, as shown in Fig. 3(e). The results show that the  $\sigma$  phase is rich in chromium and molybdenum, and another eutectoid product secondary austenite phase is rich in nickel, with less chromium than the primary austenite, which is consistent with results found in the literature [25].

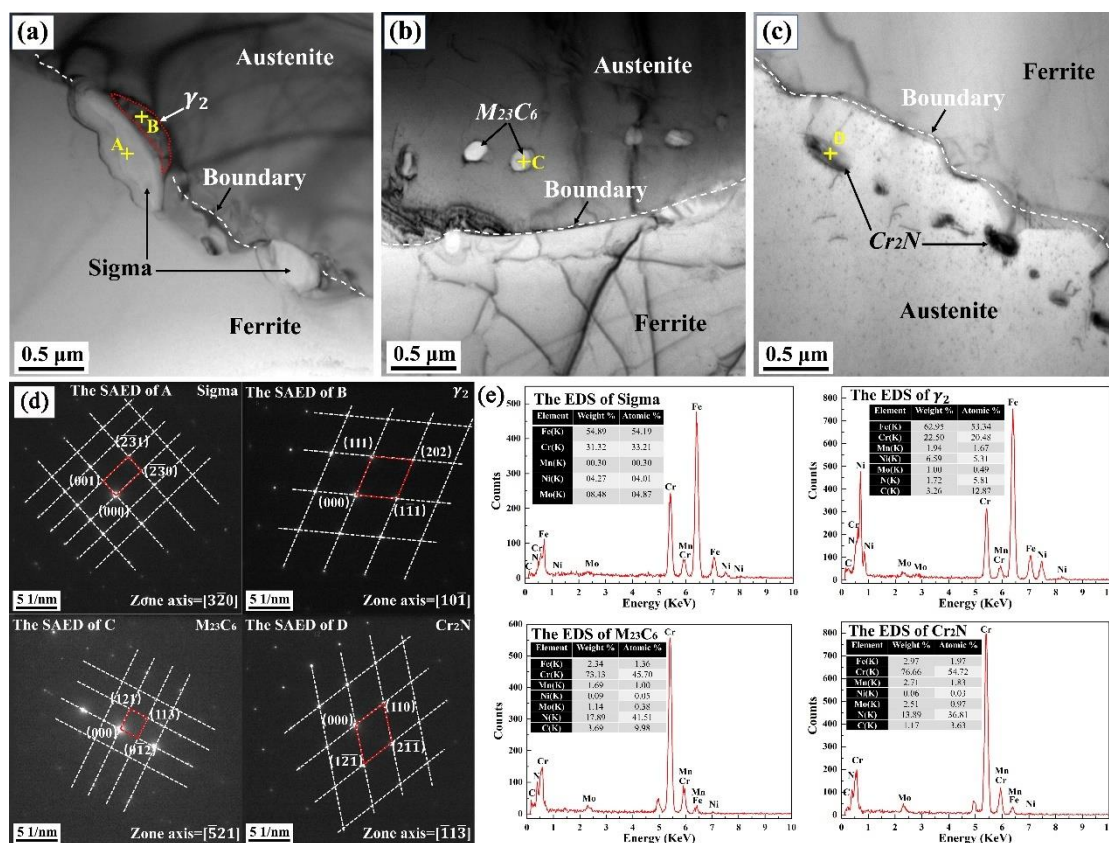


**Figure 3.** TEM results of the UNS S32750 specimens aged at 900 °C, and the corresponding selected area electron diffraction (SAED) patterns are shown in (d). The EDS spectra of the precipitates are shown in (e).

The EDS result of linear scanning along the precipitates is shown in Fig. 4. The chromium content of the precipitated phase is obviously higher than that of the  $\alpha$  and  $\gamma$  matrix, and the adjacent chromium-depleted region is approximately 100-200 nm. The active and unstable Cr-depleted zones are more likely to be attacked by chloride ions and preferentially dissolved, resulting in intergranular corrosion and pitting corrosion [26].

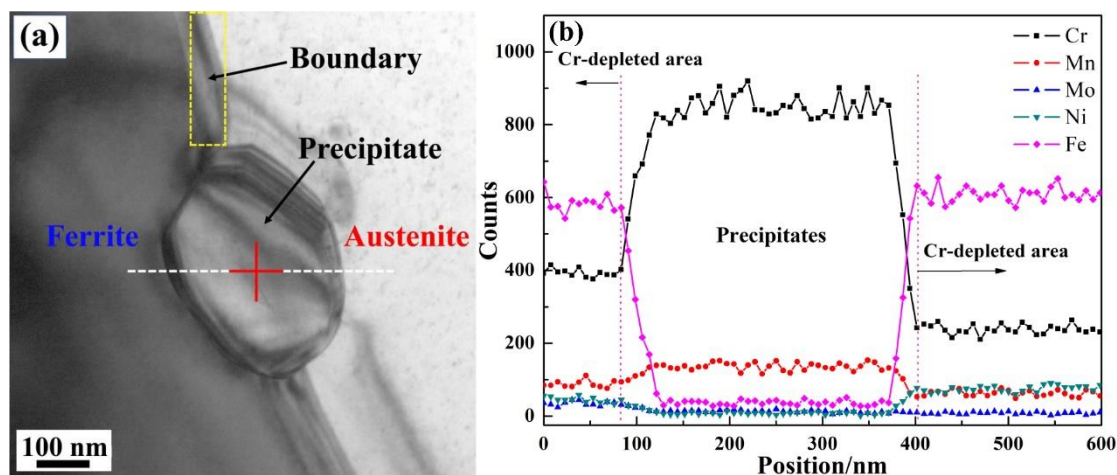


**Figure 4.** (a) High magnification TEM images of the precipitate in UNS S32750 and (b) the variation of Cr content at the marked point in (a).

### 3.2 Effect of ageing on critical pitting temperature

According to Zhang et al. [15,27], the potentiostatic critical pitting temperature measurement is a method with good reproducibility, sensitivity and efficiency that can be potentially used to evaluate the pitting resistance of stainless steel.

The typical current density versus temperature curves of ageing UNS S32750 are shown in Fig. 5. It is obvious that after several seconds of response, the current density is stable to approximately  $10^{-6}$ - $10^{-7}$  A/cm<sup>2</sup>, which means the steel is passivated. With the elevation of the electrolyte temperature, some unstable peaks appear, indicating the form of metastable pits. A sharp increase in the current density is observed as the temperature increased, which means that stable pits are generated.

It is well known that chloride ions can destroy the passive film on the surface of specimens but is accompanied by a self-healing process of the passive film [28]. When the electrolyte temperature is low, the self-repairing speed and destruction rate of the passive film can maintain a dynamic equilibrium, which makes the system metastable and forms unstable pits, however, the pits will re-passivate quickly. With the increase of electrolyte temperature, the self-repairing ability gradually weakens, and the destruction speed is much faster than the self-repairing rate; thus, the equilibrium stage is broken and the system reaches an accelerated disruption state. The formed pits continue to deepen with inward corrosion and form stable pits. At this point, the current density increases sharply [29].

Table 2 lists the average critical pitting temperatures (CPT) for different ageing times. As shown in the table, the CPT value of the as-annealed specimens is the highest because there is no precipitate phase and the material has the best corrosion resistance. With the ageing time extended to no longer than 10 h, the CPT value of the steel continues to decrease. It mainly occurs to the precipitates, especially in the  $\sigma$  phase, as discussed in the former part. The  $\sigma$  phase is Cr- and Mo- rich, which leads to a chromium-deficient area around the  $\sigma$  phase and results in deteriorated corrosion resistance. With the growth of the  $\sigma$  phase, the degree of chromium depletion will increase, and the corrosion resistance of the materials decreases. Thus, the CPT value for materials decreased with an increase of ageing time of up to 10 h. However, after further extending the ageing time, the CPT slightly increased, indicating a healing effect.

This is because the Cr-depleted regions near the precipitates are replenished with Cr atoms from the matrix [22].

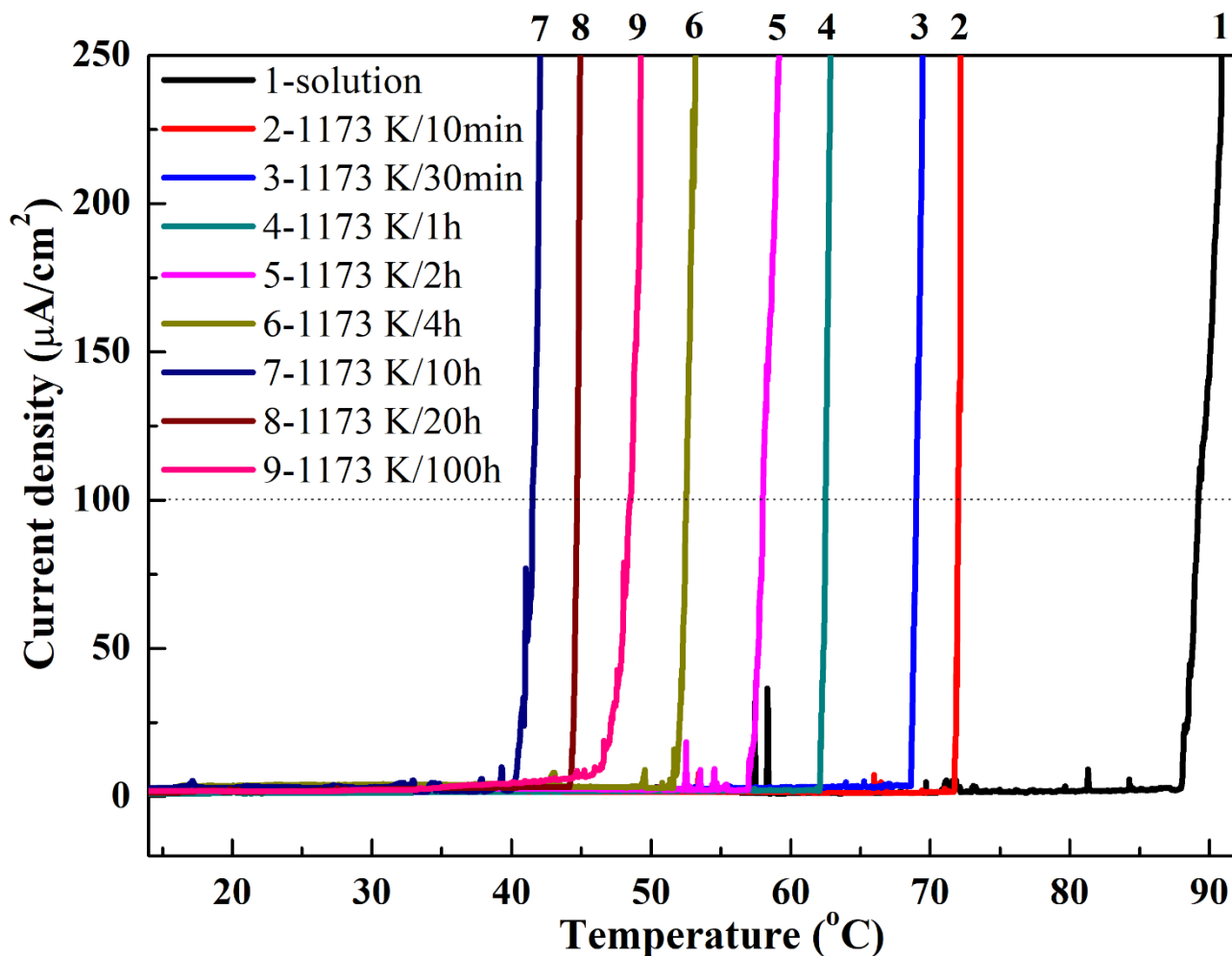


**Figure 5.** Evaluation of CPT in UNS S32750 with potentiostatic measurements at 900 °C of various sensitization times: (1) 0 min, (2) 10 min, (3) 30 min, (4) 1 h, (5) 2 h, (6) 4 h, (7) 10 h, (8) 20 h, and (9) 100 h.

**Table 2.** Critical pitting temperatures (CPT) of the UNS S32750 specimens aged at 900 °C for various times.

Specimen	1	2	3	4	5	6	7	8	9
CPT (°C)	89.2	72.0	69.0	62.5	58.0	52.5	41.5	44.7	48.0

Fig. 6 indicates the pit morphology of the as-annealed specimens and specimens aged at 900 °C for 4 h after the CPT tests. As depicted in Fig. 6(a), the pitting corrosion of the as-annealed specimens

occurs not only along the interface but also in the phase interior. As shown in Fig. 6(b-d), the pits, in the aged specimens, mainly originate from the  $\alpha/\gamma$  interface and newly produced  $\sigma/\gamma$  interface. As we discussed in the former part, the precipitate induces the chromium- and molybdenum-depleted area adjacent to them [30,31]. The lower concentration of Cr leads to the formation of a weak passive film in the Cr-depleted zones. Aggressive ions can easily penetrate through the passive film and act as a precursor for pit nucleation.

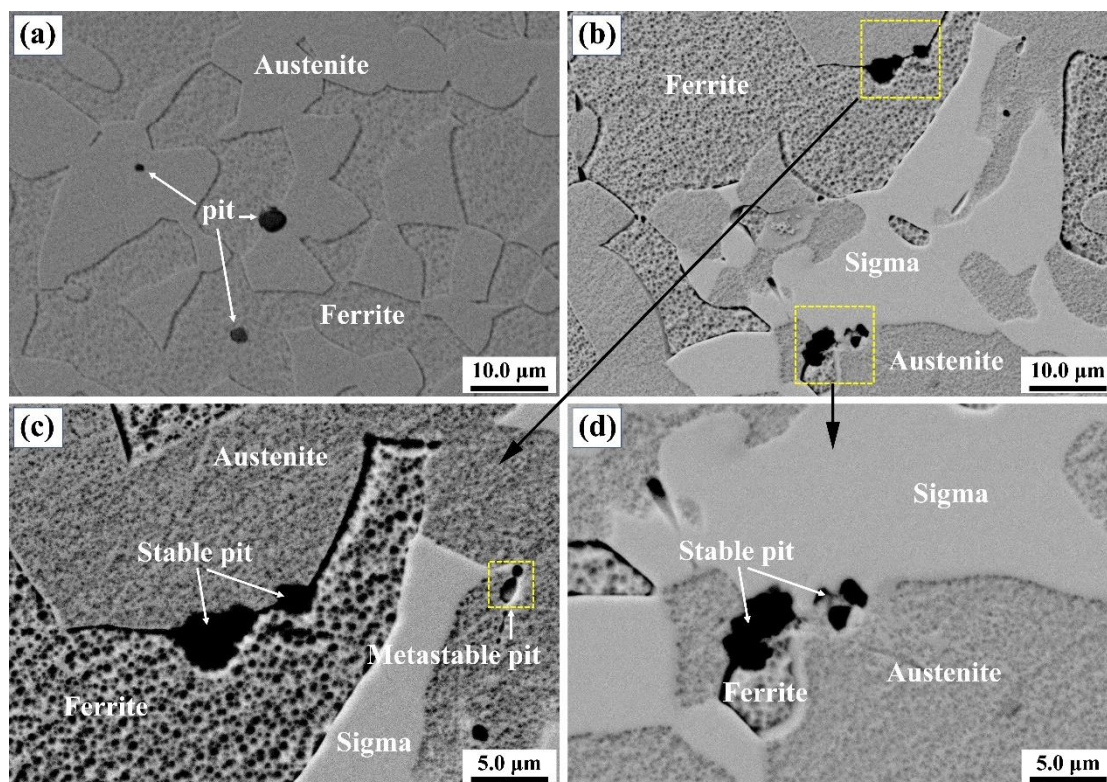


**Figure 6.** SEM-BSE pit morphologies on the surface of the specimens after CPT tests: (a) as-annealed and (b) aged at 900 °C for 4 h (Figure c and d are local magnifications of the selected areas in Figure b).

### 3.3 Degree of Sensitization (DOS) measurement

Fig. 7 shows typical DL-EPR curves of duplex stainless steels UNS S32750 after heat treatment at 900 °C for different times. The  $I_a$ ,  $I_r$  and DOS values of different specimens are listed in Table 3. The  $R_a$  values of the specimens increase with the extension of the ageing time, which means that the degree of intergranular corrosion is increasingly aggravated. The solution-annealed specimen did not exhibit a reactivation peak, which means that it had not been sensitized. The reactivation current ( $I_r$ ) value of the aged specimen increases from  $10^{-4}$  A/cm<sup>2</sup> to  $10^{-2}$  A/cm<sup>2</sup> with increasing ageing time. Although the value of the activation current ( $I_a$ ) also indicates a tendency to increase, its increase rate is much slower than the  $I_r$  value, hence showing an increasing DOS value. The reactivation peak current of specimens ageing for a short time is approximately  $10^{-4}$  A/cm<sup>2</sup>. However,  $I_r$  values of up to  $10^{-2}$  A/cm<sup>2</sup> for severely sensitized specimens (aged for 10-100 h) are due to attacks on the chromium-depleted zones adjacent to

the Cr-rich precipitates. It should be emphasized that  $I_r$  and  $I_a$  did not occur at the same potential, which is due to ohmic resistance drop [12]. It is generally known that the susceptibility to IGC of duplex stainless steel is controlled by a distribution of alloy elements in each phase [18]. During the formation of these precipitates, the elements of Cr and Mo spread from the  $\alpha$  phase to the growing  $\sigma$  phase, causing a wide range of localized Cr and Mo depletion zones around the  $\sigma$  phase. When the ageing time is extended to 100 h, the  $R_a$  value of UNS S32750 specimens increases, and there is no sign of healing.

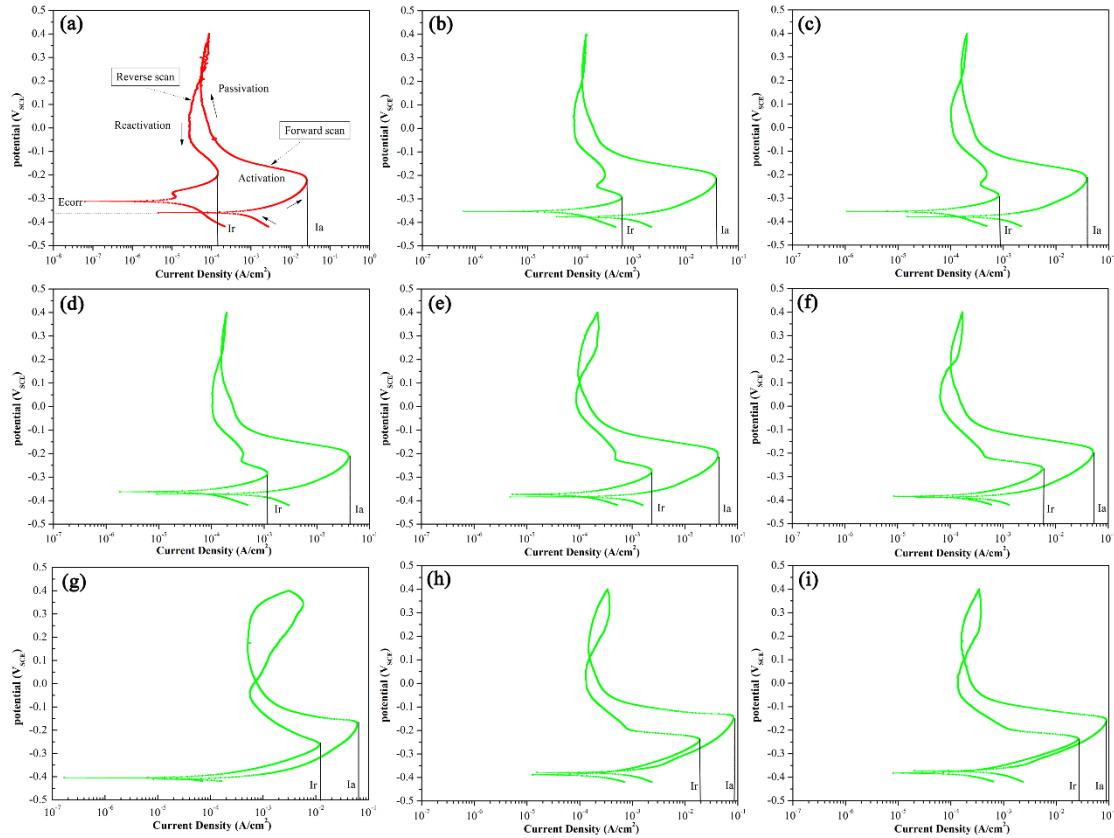


**Figure 7.** Typical DL-EPR curves of UNS S32750 aged at 900 °C for various times: (a) 0 min, (b) 10 min, (c) 30 min, (d) 1 h, (e) 2 h, (f) 4 h, (g) 10 h, (h) 20 h, and (i) 100 h.

**Table 3.** DL-EPR test results of various specimens.

Ageing conditions	Activation current $I_a$ (A/cm <sup>2</sup> )	Reactivation current $I_r$ (A/cm <sup>2</sup> )	DOS $R=I_r/I_a$
As-annealed	0.02594	1.47E-04	0.0057
900 °C -10 min	0.03777	6.11E-04	0.0162
900 °C-30 min	0.03807	8.19E-04	0.0215
00 °C-1 h	0.04026	0.00116	0.0288
900 °C-2 h	0.04282	0.00237	0.0554
900 °C-4 h	0.05162	0.00571	0.1106
900 °C-10 h	0.06165	0.01173	0.1903
900 °C-20 h	0.08295	0.01904	0.2295
900 °C-100 h	0.09001	0.02604	0.2893

Fig. 8 presents SEM photographs of the IGC attack on duplex stainless steel UNS S32750 after heat treatment at 900 °C for different times. Fig. 8(a) shows that there is no sign of intergranular corrosion in the as-annealed specimens due to the lack of a Cr-depleted region. In particular, the tendency of intergranular corrosion appears in specimens aged for 10 min ( $I_r/I_a = 1.62\%$ ). From Fig. 8(b), we can observe that phase boundaries are preferential attacks, which means the precipitates begin to generate. With the extension of ageing time, a deeper intergranular attack is obvious, as shown in Fig. 8(c-e). In addition, for specimens aged 100 h, as shown in Fig. 8(f), it is obvious that an IGC attack on the steel was most serious, which is in agreement with the DL-EPR results.

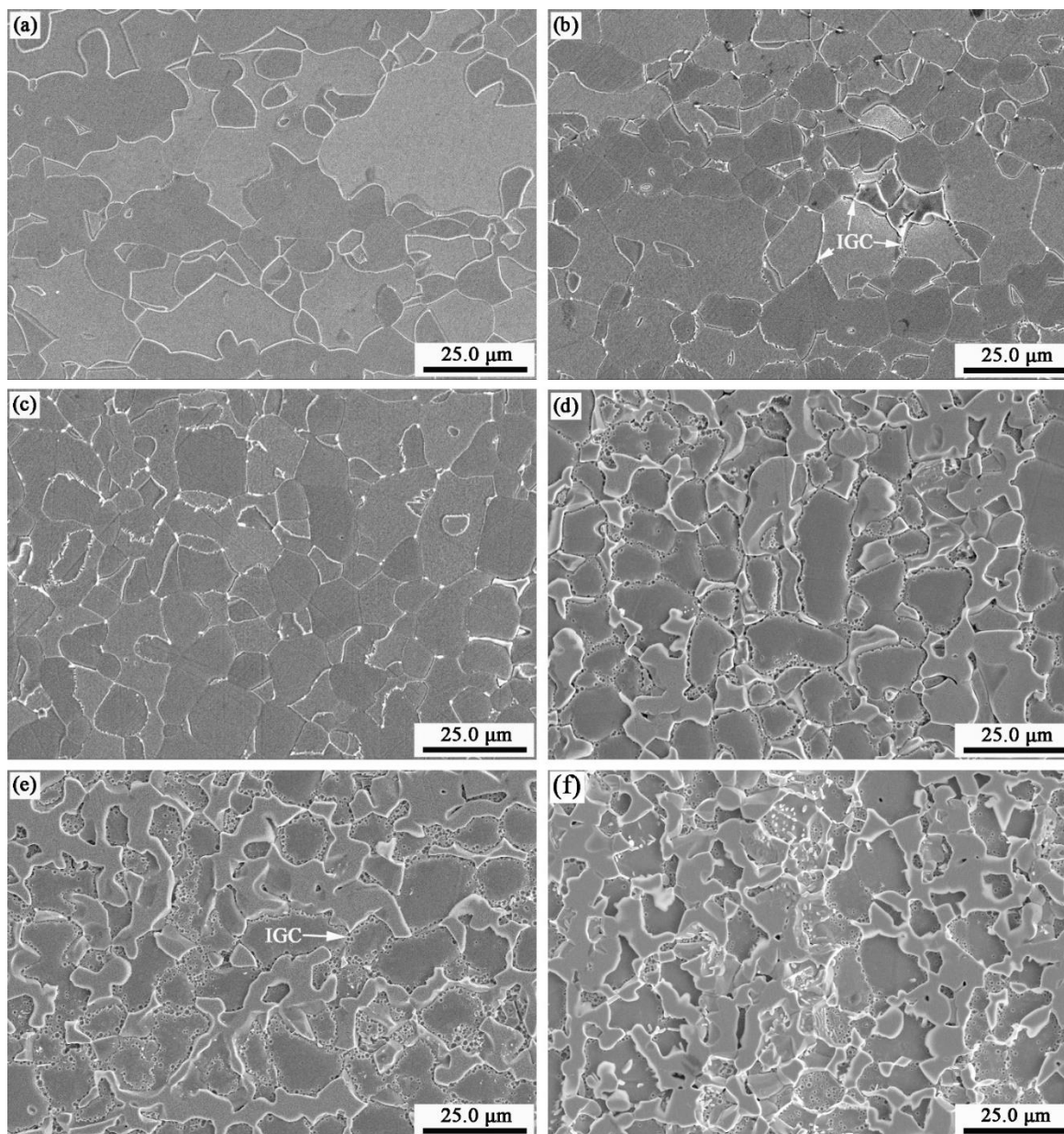


**Figure 8.** Typical micrographs after an intergranular corrosion attack on UNS S32750 aged at 900 °C for various times: (a) as-annealed, (b) 30 min, (c) 1 h, (d) 10 h, (e) 20 h, and (f) 100 h.

## 3.4 Correlation between DOS and CPT of UNS S32750

Fig. 9 indicates the correlation between the critical pitting temperature (CPT) and degree of sensitization (DOS) versus ageing time of the specimens. It is obvious that the DOS value and the CPT value initially increases and decreases, respectively. For specimens aged from 10 min to 1 h, the CPT values decrease by approximately 9.5 °C, while DOS increases by only 1.26 %. This is because the  $\sigma$  phase produced by short-term ageing induces pitting corrosion, thereby reducing the CPT value. However, the quantity of precipitates at this point are very small, and their dimensions are small; thus, the affected zones adjacent to the precipitates are small, so the sensitivity towards intergranular corrosion is not serious. This is an explanation for the obvious decrease of CPT value during the process of ageing for a short-time, while the change of DOS value is not obvious. Nevertheless, by increasing the sensitization time from 1 h to 10 h, the CPT values decrease by 21 °C, and the DOS increases from 2.88 % to 19.03 %. The remarkable change of the CPT and DOS values can contribute to the precipitate volume fraction increasing significantly. It should be noted that there is no linear relationship between CPT and DOS, as reported by Ebrahimi et al. [32], due to the complex precipitation mechanism; thus, the corrosion resistance is not only related to a single precipitate phase.

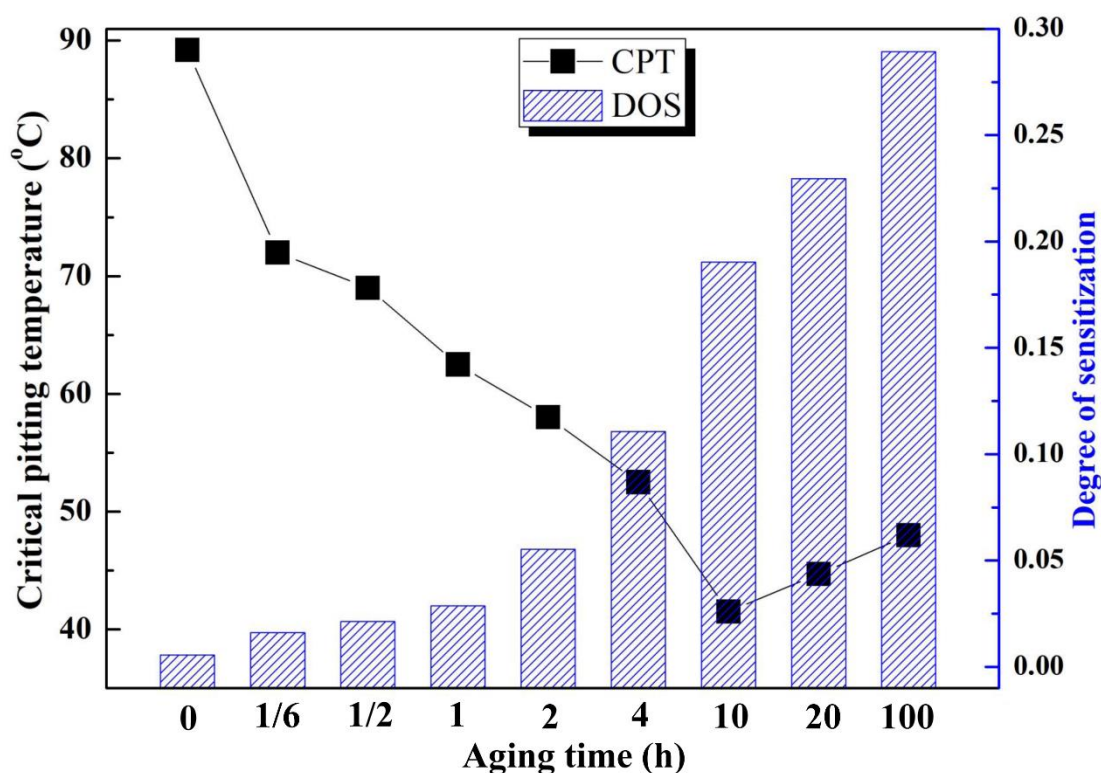


**Figure 9.** Correlation between the DOS and CPT of UNS S32750 aged at 900 °C for various times.

After extending the ageing time from 10 h to 100 h, the values of DOS continue to increase from 9.9 % to a maximum. However, the pitting corrosion resistance has an obvious healing phenomenon because most of the ferrite has transformed, and the dominant mechanism will be the chromium

replenishment effect. Therefore, the pitting resistance is enhanced, which causes the CPT value to slightly increase again, and the above results are consistent with Somogyi's report [33]. However, for the DOS evaluation technique, it is affected not only by the weakest area but also by the entire area of the specimen.

#### 4. CONCLUSIONS

A correlation between the CPT and DOS combined with a microstructure evolution analysis of S32750 aged at 900 °C for different durations was investigated. The main conclusions are as follows:

1. A microstructural analysis of DSS UNS S32750 showed that with increasing aging time, the ferrite volume fraction decreased and the precipitate volume fraction increased. The main precipitates are  $\sigma$  and  $\text{Cr}_2\text{N}$ . The precipitation mechanism is  $\alpha \rightarrow \sigma + \gamma_2$  and  $\alpha \rightarrow \text{Cr}_2\text{N} + \gamma_2$ .

2. The results demonstrated that both the CPT and DOS are strongly dependent on the microstructure.

3. A significant deterioration of pitting corrosion resistance was found after ageing for 10 min, but intergranular corrosion sensitivity increased slightly after short-term ageing.

4. With a prolonged ageing time of 100 h, the pitting resistance was healed, but the degree of sensitization (DOS) continued to increase.

#### ACKNOWLEDGMENTS

The author would like to thank KaiWei Wu for his great help with characterization of the specimen. This work is supported by the National Science Foundation of China (No. 11604204).

#### References

1. D. Kang, N. Kim, H. Lee, *Met. Mater. Int.*, 25(2019)740
2. Z. Zhang, H. Zhao, H. Zhang, Z. Yu, J. Hu, L. He, J. Li, *Corros. Sci.*, 93(2015)120
3. Z.Y. Cui, S. Chen, Y.P. Dou, S.K. Han, L.W. Wang, C. Man, X. Wang, S. Chen, Y.F. Cheng, X. Li, *Corros. Sci.*, 150(2019)218
4. R.G. Laycock, T.H. Fletcher, *Fuel. Process. Technol.*, 175(2018)35
5. N. Kauss, A. Heyn, T. Halle, P. Rosemann, *Electrochim. Acta*, 317(2019)17
6. A.K. Lakshminarayanan, V. Balasubramanian, *Mater. Design*, 39(2012)175
7. H. Shaikh, N. Sivaibharasi, B. Sasi, T. Anita, R. Amirthalingam, B.P.C. Rao, T. Jayakumar, H.S. Khatak, Baldev Raj, *Corros. Sci.*, 48(2006)1462
8. M. Scohy, L. Dubau, C. Montella, F. Claudel, S. Abbou, *Electrochim. Acta*, 320(2019)134536
9. J. Yang, J. Shao, L. Wu, Y. Li, X.D. Zhao, S.A. Wang, D.Y. Sun, J. Sun, *Int. J. Electrochem. Sci.*, 14(2019)9193
10. Y.H. Liew, D.J. Blackwood, S. Wijesinghe, *J. Electrochem. Soc.*, 166(2019)410
11. H.T. Yan, S.S. Xin, Y. Yang, S. Yang, M.C. Li, *Int. J. Electrochem. Sci.*, 14(2019)1423
12. P.Z. Cheng, N. Zhong, N.W. Dai, X. Wu, J. Li, Y.M. Jiang., *J. Mater. Sci. Technol.*, 35(2019)1787
13. Y. Zhao, Y. Wang, S.A. Tang, W.N. Zhang, Z.Y. Liu, *J. Mater. Process. Tech.*, 266(2019)246

14. J. R. Carrasco, U. Krupp, V.H. L. Morelos, A. Giertlerb, M.A.G. Rentería, J.G. Sánchez, *Int. J. Fatigue*, 121(2019)243
15. S.C. Zhang, Z.H. Jiang, H.B. Li, H. Feng, B.B. Zhang, *J. Alloy. Compd.*, 695(2017)3083
16. H. Wang, X. Zhang, G.B. Wang, J. Shen, G.Q. Zhang, Y.P. Li, M. Yan, *J. Alloy. Compd.*, 807(2019)151662
17. M.L. Wang, H.Z. Cui, Y.Q. Zhao, C.M. Wang, N. Wei, Y. Zhao, X. Zhang, Q. Song, *Mater. Design*, 180(2019)107893
18. M. Akashi, T. Kawamoto, F. Umemura, B. Gijutsu, *Corros. Eng.*, 29(1980)163
19. X.J. Qin, X.L. Guo, J.Q. Lu, L.Y. Chen, J.I. Qin, W.J. Lu, *J. Alloy. Compd.*, 698(2017)1094
20. B. Deng, Y.M. Jiang, J.L. Xu, T. Sun, J. Gao, L.H. Zhang, W. Zhang, J. Li, *Corros. Sci.*, 52(2010)969
21. Z.Q. Feng, Y.H. Yang, J. Wang, *J. Alloy. Compd.*, 699(2017)334
22. I. Calliari, M. Pellizzari, M. Zanellato, E. Ramous, *J. Mater. Sci.*, 46(2011)6916
23. C.T. Kwok, K.H. Lo, W.K. Chan, F.T. Cheng, H.C. Man, *Corros. Sci.*, 53(2011)1581
24. J. Gong, Y.M. Jiang, B. Deng, J.L. Xu, J.P. Hu, J. Li, *Electrochim. Acta*, 55(2010)5077
25. A. Bhattacharya, P.M. Singh, *Corrosion*, 64(2008)532
26. C. Man, C.F. Dong, D.C. Kong, L. Wang, X.G. Li, *Corros. Sci.*, 151(2019)108
27. Z. Zhang, H. Zhang, H. Zhao, J. Li, *Corros. Sci.*, 103(2016)189
28. M. Motamedi, M. Ramezanzadeh, B. Ramezanzadeh, S. Saadatmandi, *Appl. Surf. Sci.*, 488(2019)77
29. Q.C. Wang, B.C. Zhang, Y.B. Ren, K. Yang, *Corros. Sci.*, 145(2018)55
30. H. Tan, Y. Jiang, B. Deng, T. Sun, J. Xu, J. Li, *Mater. Charact.*, 60(2009)1049
31. B. Deng, Y.M. Jiang, J. Gao, J. Li, *J. Alloy. Compd.*, 493(2010)461
32. N. Ebrahimi, M. Momeni, M.H. Moayed, A. Davoodi, *Corros. Sci.*, 53(2011)637
33. A. Somogyi, A. Horvath, G. Nagy, *Corrosion*, 67(2011)6

© 2020 The Authors. Published by ESG ([www.electrochemsci.org](http://www.electrochemsci.org)). This article is an open access article distributed under the terms and conditions of the Creative Commons Attribution license (<http://creativecommons.org/licenses/by/4.0/>).